JOURNAL OF GUIDANCE, CONTROL, AND DYNAMICS
Vol. 24, No. 5, September–October 2001

Bifurcation Analysis of Attitude Dynamics in Rigid Spacecraft with Switching Control Logics

Giulio Avanzini*
Polytechnic of Turin, 10129 Turin, Italy
and
Guido de Matteis†
University of Rome "La Sapienza," 00184 Rome, Italy

A numerical continuation method is used for bifurcation analysis of the complex behavior that appears in the attitude dynamics of rigid spacecraft as a result of switching logics in control system elements. Because the stability analysis of limit cycles is carried out in most circumstances, the application of the continuation method raises a number of issues when such aspects as nonlinearities that can not be approximated by differentiable functions and noninvertible input–output relations are taken into consideration. An approach based on the continuation of equilibrium points of the Poincaré map for the analysis of dynamic systems with motion-dependent discontinuities is presented. Spacecraft configurations featuring single-axis control loops are investigated, where momentum wheels or reaction thrusters are used. In the latter case, the characterization of the dynamic behavior of a pulse-modulated control system is used as an example of the proposed methodology. The results show that the considered configurations can be successfully analyzed by the continuation technique, without performing extensive numerical simulation.

Nomenclature

$\boldsymbol{F}$	=	Poincaré map
$\boldsymbol{f}$	=	vector field
g	=	switching function
h	=	angular momentum
I_y	=	pitch moment of inertia
K	=	modulator filter gain
K_p, K_i, K_d	=	proportional, integral, and derivative feedback gains
$\boldsymbol{M}$	=	manifold in the state space
m	=	parameter space dimension
n	=	state-space dimension
$\boldsymbol{P}$	=	Poincaré section
t	=	time
U	=	control torque
U_m	=	thruster torque
$U_{\max}$	=	maximum torque
v	=	Schmitt trigger filter variable
v_{on}, v_{off}	=	Schmitt trigger switching thresholds
$\boldsymbol{x}$	=	state vector
y	=	integrator variable
δt	=	time increment
$\epsilon_{\max}$	=	integrator reset threshold
ζ	=	closed-loop damping
θ	=	pitch angle
λ	=	continuation parameter
$\boldsymbol{\mu}$	=	parameter vector
τ	=	modulator filter time constant
τ_E	=	motor time constant
τ_i	=	reset time constant
ω	=	angular velocity
ω_n	=	closed-loop bandwidth

Subscripts

com	=	commanded
e	=	at equilibrium
M	=	at intersection with manifold $\boldsymbol{M}$
max	=	maximum
0	=	initial condition

Presented as Paper AAS 99-150 at the AAS/AIAA Space Flight Mechanics Meeting, Breckemridge, CO, 7–10 February 1999; Received 1 November 1999; revision received 28 August 2000; accepted for publication 29 December 2000.

*Research Scientist, Department of Aeronautical and Space Engineering, corso Duca degli Abruzzi 24. Member AIAA.

†Professor, Department of Mechanics and Aeronautics, Via Eudossiana 18. Member AIAA.

I. Introduction

SPACECRAFT performance specifications require high attitude pointing accuracy during nominal modes of operation. In recent years, the presence of nonlinearities in both the actuation devices and the control laws has raised increasing concerns, as a cause of degradation of the system performances and, in certain circumstances, as a source of instability. Note the adverse effects of saturation, hysteresis, and time delay in the actuator characteristics,[1] as well as the unwanted consequences of nonlinearities contained in control system elements. In the latter situation, for instance, there are subsystems such as relays with hysteresis and deadzone or variable-structure, proportional plus integral (PI) regulators incorporating antiwindup reset that are usually featured in reaction or in momentum wheel speed controllers, respectively. The analysis of controlled systems containing the aforementioned nonlinear elements may show a complex behavior where periodic, quasi-periodic, subharmonic, and chaotic motions are present.

The describing function method[2] (DFM) deserves consideration in control system analysis because it allows the prediction of the frequency and amplitude of limit cycles when the behavior of a basically linear system is characterized by the presence of nonlinear algebraic elements in the control laws and/or in the actuator dynamics. Nevertheless, DFM is inherently inexact as a means of accurately analyzing complex dynamic phenomena. In a different approach,[3] where the use of DFM to designate nonlinear stability margins in pulse-modulated control system design is demonstrated, the oscillation characteristics of the system cannot be accurately identified. The problem of checking the presence or absence of limit cycles in face of parametric uncertainties is addressed in Ref. 4 for a closed-loop system containing a linear time-invariant transfer function and a separable autonomous nonlinear element. In that study,[4] a structured singular-value-based method is used, in the DFM context of first harmonic approximation.

Dynamic system theory[5] (DST) provides a powerful tool for the analysis of nonlinear systems. In the framework of DST, bifurcation analysis has been widely used to study the nonlinear behavior of both uncontrolled and controlled systems in the aerospace field. Among many works on the subject, in Ref. 6, catastrophic jump phenomena

are investigated for various types of nonlinear elements in a control system subjected to a sinusoidal input, and in Ref. 7, a nonlinear, time-periodic system, stabilized by a modal control scheme is examined using Poincaré maps. In Ref. 8, where a single input/single output (SISO), pitch axis control system of a momentum-biased satellite is dealt with, a global analysis is carried out by numerical simulation to illustrate, by means of Poincaré mapping, the effect of the motor time constant on the system behavior that involves multiple limit cycles and strange attractors. Extensive simulation is required in Refs. 7 and 8 to generate Poincaré maps and to locate accurately bifurcation points. However, even though in most cases the logic of the controller is simple in design for the sake of reliability, the presence of regions in the parameter space, where the qualitative behavior of the dynamic system presents relevant variations, may not be identified by simulation,[1] due to the high number of system parameters involved.

In this paper, a novel approach is proposed for the bifurcation analysis of the attitude dynamics of spacecraft configurations where discontinuous or nonsmoothed characteristics of the control system determine limit-cycling conditions. The method is based on numerical continuation[9] of Poincarè map equilibria for the vehicle model and allows complex nonlinear phenomena observed in closed-loop attitude dynamics, as well as the effects of design parameters of the control system, to be investigated efficiently without performing extensive numerical simulations. When two significant applications to single-axis stabilized spacecraft are considered, the analysis is also intended to unfold those situations where the application of the technique appears less effective or not appropriate.

The use of a numerical continuation algorithm in the analysis of spacecraft attitude control system raises a number of specific issues that are not given due attention in the reported applications. First, it is apparent that small-amplitude, self-sustained oscillations may be the unwanted result of reset logic and torque saturation in a momentum bias configuration[8] or may constitute the normal mode of operation induced by the switching logic of a pulse modulator as well. The use of a continuation algorithm for limit-cycle analysis requires that the system under consideration be in the general form

$$\dot{\boldsymbol{x}} = \boldsymbol{f}(\boldsymbol{x}, \boldsymbol{\mu}) \tag{1}$$

where $\boldsymbol{x} \in \boldsymbol{R}^n$ is the state vector, $\boldsymbol{\mu} \in \boldsymbol{R}^m$ is a vector of parameters, and $\boldsymbol{f} : \boldsymbol{R}^n \times \boldsymbol{R}^m \to \boldsymbol{R}^n$ is a nonlinear C^1 continuous vector field.[9] In satellite configurations featuring switching logic in the control system, the C^1 approximation of discontinuous functions becomes a critical issue because the qualitative behavior of the system may not be preserved once the smoothing is accomplished.

The second problem is more subtle and concerns the use of continuation methods in the analysis of reaction controllers. As a significant example, consider pulse modulators based on the well-known Schmitt trigger, where a vertical jump of the trigger output $u(t)$ occurs whenever the input $v(t)$ crosses the switching thresholds of the relay hysteresis band. Therefore, the trigger has the highly nonlinear input–output relation $u(t) = g[v(t), v(t-\delta t)]$ (Ref. 10), that prevents the system from being formulated in the form of Eq. (1). Note also that g cannot be approximated by a differentiable (at least) function.

In spite of the limitations, the continuation technique can still be used provided that an approach based on the concepts of Poincaré map and discrete-time systems is adopted where, as a major advantage, the continuity of the vector field $\boldsymbol{f}$ in the whole phase space $\boldsymbol{R}^n$ is not required. In particular, we assume that system (1) is continuous only in defined regions of $\boldsymbol{R}^n$ separated by $(n-1)$-dimensional manifolds and apply the continuation method to calculate the steady-state solutions and bifurcation points of the discrete system

$$\boldsymbol{x}_{k+1} = \boldsymbol{F}(\boldsymbol{x}_k, \boldsymbol{\mu}) \tag{2}$$

where $\boldsymbol{F} : \boldsymbol{P} \times \boldsymbol{R}^m \to \boldsymbol{P}$ is the Poincaré map, $\boldsymbol{P} \subset \boldsymbol{R}^n$ is the Poincaré section of dimension $n-1$, and $\boldsymbol{x}_k \in \boldsymbol{P}$. The map $\boldsymbol{F}$ is determined by analytical or numerical computation of the solution curves of the spacecraft equations of motion, between two successive intersections with $\boldsymbol{P}$. To this end, the discontinuities are detected, and the time value when the discontinuity occurs is accurately evaluated.

To discuss the advantages and possible limits of our approach, two SISO rigid systems are analyzed, where nonlinear elements with switching logics are present in the control laws. Unlike Ref. 7, where linear control laws are applied to a nonlinear system, we have linear dynamics in the uncontrolled satellite model. This approach, also adopted in Ref. 8, allows a detailed investigation of the effects of the control loop nonlinearities and a sound evaluation of the proposed methodology as well because complicated dynamics of the open-loop plant are omitted. Furthermore, practical applications such as the validation of control logics are not ruled out by the assumption of a linear open-loop model due to the small perturbations involved in the motion of the controlled system. In particular, we consider 1) a PI compensation network with integrator reset and wheel torque saturation (model 1) and 2) a proportional–derivative (PD) network including a pulse-width pulse-frequency (PWPF) thruster modulator,[11] where both the width of the activated reaction pulse and the distance between the pulses are modulated proportionally to the error level (model 2).

The former configuration, already considered in Ref. 8, is recalled for comparing and validating the results of the present method. In the second application, which lends itself for the analytical determination of the Poincaré map $\boldsymbol{F}$, bifurcation theory provides a way of validating the control laws, as determined by a classical design process and investigating the behavior of the system as the controller parameters are varied.

The proposed approach is described in detail in Sec. II. Then, Secs. III and IV are dedicated to the analysis of the SISO configurations corresponding to model 1 and 2, respectively. A section of conclusions ends the paper.

II. Limit-Cycle Analysis

In this section, we present our technique for tracing branches of limit cycles using continuation of equilibrium solutions of the Poincaré map. See the work of Guckenheimer and Holmes[5] for the definitions of equilibrium point, periodic solution, and discrete map. A detailed description of the continuation algorithm is reported in Refs. 12 and 13.

As observed in Sec. I, the vector field $\boldsymbol{f}$ of the considered spacecraft configuration can not be approximated by continuous functions due to the presence of the aforementioned nonlinearities in the control laws. Nevertheless, provided that $\boldsymbol{f}$ exhibits periodic solutions, the pertinent Poincaré map $\boldsymbol{F}$ is at least locally continuous with respect to variations of initial conditions and system parameters.[5] Therefore, the bifurcation analysis can be performed in terms of numerical continuation[9] of the equilibrium solutions of Eq. (2), and we write

$$\boldsymbol{x}_{k+1} = \boldsymbol{x}_k + \int_{t_k}^{t_{k+1}} \boldsymbol{f}(\boldsymbol{x}, \boldsymbol{\mu})\, \mathrm{d}t \tag{3}$$

where the orbit period $T = t_{k+1} - t_k$ is to be evaluated. In this study, $\boldsymbol{x}_{k+1}$ is calculated numerically by a fourth-order Runge–Kutta integration algorithm for model 1 and analytically for model 2. To determine T, a secant iteration scheme is used to locate the value of the time when the section $\boldsymbol{P}$ is intersected. In particular, an intersection is detected when $|x_i|/||\boldsymbol{x}|| \leq 10^{-6}$, where x_i is the ith element of the state vector and $x_i = 0$ is the Poincaré section.

Note that the Poincaré map is to be continuous with respect to variations of both $\boldsymbol{x}_k$ and $\boldsymbol{\mu}$ for the application of the continuation method. In this respect we recall that a solution curve emanating from a point $\boldsymbol{x}_0$ of the phase space can be represented in terms of phase flow ϕ, that is, $\boldsymbol{x} = \phi(\boldsymbol{x}_0, t - t_0)$, where $\boldsymbol{x}$ is a smooth function of both $\boldsymbol{x}_0$ and t, when the vector field $\boldsymbol{f}$ is continuous.[5,14] If a vector field with a discontinuity on a manifold $\boldsymbol{M}$ is considered, it is possible to divide the phase space into two regions where the vector field is continuous. Thus, the phase flow can be represented by two locally continuous flows ϕ_1 and ϕ_2, on the two sides of $\boldsymbol{M}$, connected by the function $\sigma : \boldsymbol{M} \to \boldsymbol{M}$ that describes the action of the discontinuity on the system state. The solution curves that intersect $\boldsymbol{M}$ are, thus, split into three sections in the phase space as 1) a first path, for $t_0 \leq t < t_M$, from $\boldsymbol{x}_0$ up to the point of intersection $\boldsymbol{x}_M^{(-)}$ with $\boldsymbol{M}$, such that $\boldsymbol{x}_M^{(-)} = \phi_1(\boldsymbol{x}_0, t_M - t_0)$; 2) a jump on $\boldsymbol{M}$, governed by the nature of the discontinuity and represented by the relation $\boldsymbol{x}_M^{(+)} = \sigma(\boldsymbol{x}_M^{(-)})$;

and 3) a trajectory emanating from $\boldsymbol{x}_M^{(+)}$, that is, $\boldsymbol{x}_1 = \phi_2(\boldsymbol{x}_M^{(+)}, t - t_{M_{\phi_1}})$, for $t > t_M$. Provided that σ is continuous on $\boldsymbol{M}$, the sequence $\boldsymbol{x}_0 \mapsto \boldsymbol{x}_M^{(-)} \overset{\sigma}{\mapsto} \boldsymbol{x}_M^{(+)} \overset{\phi_2}{\mapsto} \boldsymbol{x}_1$ generates a continuous phase flow with respect to the initial condition $\boldsymbol{x}_0$, although the continuity in t is no longer retained. The flow continuity for variation of a system parameter can be demonstrated in a similar fashion.[14]

Therefore, when motion-dependent discontinuities in the vector field are present, the computation of $\boldsymbol{x}_{k+1}$ and T is split in several phases, each one ending on a discontinuous manifold. A numerical algorithm for solving dynamic systems with discontinuities was presented in Ref. 15. In the same framework, we accurately determine the location $\boldsymbol{x}_M^{(-)}$ of the intersection and the crossing time t_M using a secant method, where a convergence criterion similar to that adopted for the detection of Poincaré section crossing is to be satisfied, that is, $d(\boldsymbol{x}_M^{(-),j}, \boldsymbol{M})/\|\boldsymbol{x}_M^{(-),j}\| < 10^{-8}$, where $d(\cdot,\cdot)$ is the distance between the manifold $\boldsymbol{M}$ and the jth approximation of the intersection point.

For the equilibrium points of Poincaré maps, recall that the continuation algorithm can accurately locate folds, Naimark–Sacker (the discrete version of the Hopf bifurcation) and pitchfork bifurcations, including branch switching in the latter case. These three situations correspond, respectively, to a saddle-node bifurcation, a period doubling bifurcation, and a limit-cycle splitting on a branch of periodic solutions of the continuous-time system. On the other hand, because the discrete system (2) is not Lipschitz-continuous,[5] nonstandard bifurcation points may exist that are not detected during continuation. In these circumstances, as we will see in the next section, the computation of bifurcating branches also fails because the Jacobian $\nabla \boldsymbol{F}$ (Ref. 12), evaluated by centered differences, is ill conditioned or cannot be determined with the necessary accuracy, when, for instance, a relevant variation of the phase flow occurs due to the bifurcation itself.

III. PI Network for Momentum Wheel Control

We consider a momentum-biased satellite, controlled in pitch by a simple, variable-structure compensator. The configuration, model 1, is shown in Fig. 1 and features, as nonlinear elements, the reset logic of the integrator and the torque saturation of the momentum wheel motor. Continuation of steady states and periodic solutions is carried out for trajectories in the neighborhood of the origin, that is, when the pitch error magnitude $|\epsilon|$ is smaller than the specified threshold $\epsilon_{\max}$ and the compensator has a PI structure. On the other hand, the bifurcation analysis is conducted by continuation of the Poincaré map equilibria, as outlined in the preceding section, when the controller structure is switching between PI mode and just proportional mode. In this latter situation, the requirement for C^1 continuity of the vector field $\boldsymbol{f}$ in Eq. (1) can not be met because it is not possible to smooth the integrator reset function without altering the compensating characteristics of the controller.

Formulation

The pitch axis equations of motion of the rigid system, developed in Ref. 8 for external torque $U_d = 0$, are

$$\dot{\omega} = -U/I_y, \qquad \dot{\theta} = \omega, \qquad \dot{y} = \theta g(\theta) - [1 - g(\theta)]y/\tau_i \tag{4}$$

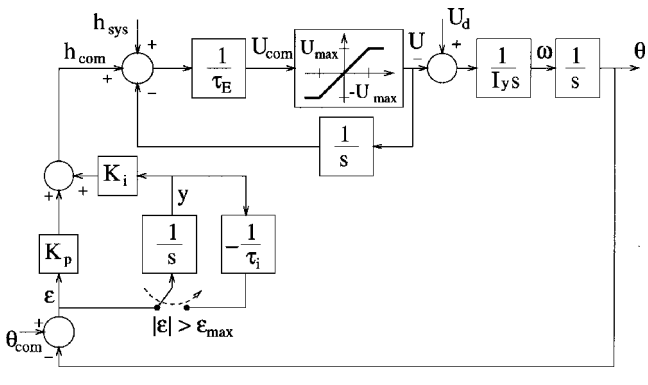

Fig. 1 Block diagram of model 1.

where $\tau_i \to 0$ for an instantaneous reset. In Fig. 1, the commanded momentum h_{com} and the nominal momentum of the system h_{sys} are also indicated. The function $g(\theta)$ in Eqs. (4) represents the integrator reset as

$$g(\theta) = 1, \qquad \text{for} \qquad |\theta - \theta_{\text{com}}| \le \epsilon_{\max}$$

$$g(\theta) = 0, \qquad \text{for} \qquad |\theta - \theta_{\text{com}}| > \epsilon_{\max}$$

where $\epsilon_{\max}$ is the switching threshold. The control torque U is

$$U = U_{\text{com}}, \qquad \text{for} \qquad |U_{\text{com}}| \le U_{\max}$$

$$U = \text{sign}(U_{\text{com}})U_{\max}, \qquad \text{for} \qquad |U_{\text{com}}| > U_{\max}$$

where

$$U_{\text{com}} = [I_y\omega + K_p(\theta - \theta_{\text{com}}) + K_i y]/\tau_E$$

The state vector of system (4) is $\boldsymbol{x} = (\omega, \theta, y)^T$ with a stable steady-state $\boldsymbol{x}_e = (0, 0, 0)^T$. The Poincaré section $\boldsymbol{P}$ is the half-plane $\omega = 0, \theta > 0$, and, as mentioned, the Poincaré map is determined by numerical integration of set (4).

Analysis

The constant parameters for model 1 are reported in Table 1. In Ref. 8, the same spacecraft configuration is investigated, and an extensive parametric study is carried out to obtain a qualitative bifurcation diagram, where the regions of attraction of multiple competing attractors and the critical values of the bifurcation parameter $1/\tau_E$, with τ_E the motor time constant, are evaluated by numerical simulation.

The global analysis is presented in Fig. 2, where the bifurcation diagram of the limit-cycle amplitude $\theta_{\max}$ is traced as a function of $\lambda = 1/\tau_E$. The subcritical Hopf bifurcation (HB) is correctly identified at $\lambda = 0.025\ \text{s}^{-1}$, and the branch of unstable limit cycles originating from the HB represents the boundary of the attracting basin for the stable steady state at the origin.

Table 1 Nominal design parameters of the satellite configurations

Parameter	Model 1[8]	Unit	Model 2[11]	Unit
I_y	1,088	kg m^2	500	kg m^2
ω_n			1.0	rad s^{-1}
ζ			1.0	
K_p	78.7	N · m s rad^{-1}	$\omega_n^2 I_y$	N · m rad^{-1}
K_d			$2\zeta\omega_n I_y$	N · m s rad^{-1}
K_i	1.97	N · m rad^{-1}		
$\epsilon_{\max}$	0.0873	rad		
$U_{\max}$	0.113	N · m		
U_m			9.5	N · m
τ_E	23	s		
v_{on}			1.0	
v_{off}			0.1	
K			2.0	(N · m)$^{-1}$
τ			0.5	s

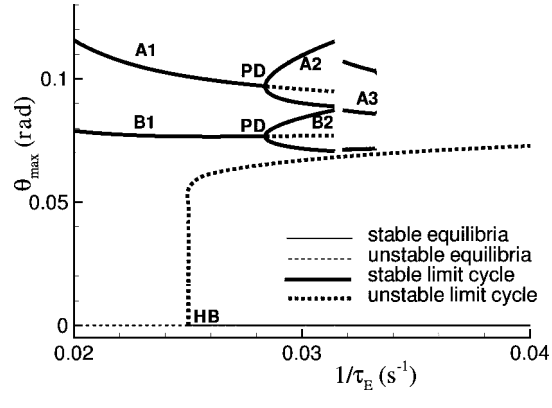

Fig. 2 Model 1: bifurcation diagram of pitch angle $\theta_{\max}$ vs $1/\tau_E$.

For the continuation of the discrete-time system represented by equilibrium points of the Poincaré map (Fig. 2), A1 and B1 indicate branches of stable and unstable periodic solutions, where the period varies from $T = 180$ s at $\lambda = 0.022$ s^{-1} to $T = 160$ s for $\lambda = 0.032$ s^{-1}. From the period doubling bifurcation (PD) at $\lambda = 0.028$ s^{-1}, the two branches of solutions of double period A2 and B2 were traced by continuation of equilibrium points of the $\boldsymbol{F}^2$ Poincaré map. The branch A3 is a stable limit cycle following the merging of the branches A2 and B2, also reported in Ref. 8. This circumstance, where two intersecting branches of periodic solutions combine into a single limit cycle with two subharmonics, could never occur in a smooth dynamic system.[5] As a consequence, we have a type of bifurcation that is not detected by the continuation method, and to trace the branch A3, it is necessary to restart the continuation after a periodic solution on that branch is determined by numerical simulation. Finally, for $\lambda > 0.034$ s^{-1}, periodic solutions disappear, and an irregular behavior, such as quasi-periodic or chaotic motion, occurs.

As a conclusion, comparison to the result of Ref. 8 shows that, in the λ range where at least one periodic solution exists, all of the solution branches for system (4) are accurately detected using a very limited number of simulations and, more importantly, all of the bifurcation points are precisely identified by the application of the continuation technique to either the continuous-time system or the Poincaré map.

IV. PD Network with Thruster Pulse Modulation

In this section, a pitch axis control loop incorporating a PWPF modulator is dealt with, the detailed description of which may be found in Ref. 11. The standard realization of the control system for pitch axis stabilization (model 2) is shown in Fig. 3, where the nonlinear element is the relay with hysteresis and deadzone (Schmitt trigger) in the modulator.

Recall that the static characteristics of the modulator are usually considered sufficient for control design of rigid spacecraft.[3] However, that approach fails to represent adequately the asymptotic behavior of the system when the error magnitude is small, and the crucial effect of finite amplitude pulses on the limit-cycling spacecraft dynamics is missed because the averaged output of the modulator is expected to be nearly linear with respect to constant input amplitude.

Our application, where the dynamic characteristics of the PWPF logic are dealt with, provides an accurate and detailed description of the oscillatory characteristics of the rigid spacecraft during nominal operation and can also be regarded as a first step in the process of pulse-modulated control system analysis and design for flexible satellites. Because, as already outlined in Sec. I, the modulator cannot be modeled as a continuous-time system of class C^1, the analysis is developed using Poincaré mapping.

Formulation

The governing equations of the rigid spacecraft model are

$$\dot{\omega} = U/I_y, \qquad \dot{\theta} = \omega$$

$$\dot{v} = \{K[K_p(\theta_{\text{com}} - \theta) - K_d\omega - U] - v\}/\tau \tag{5}$$

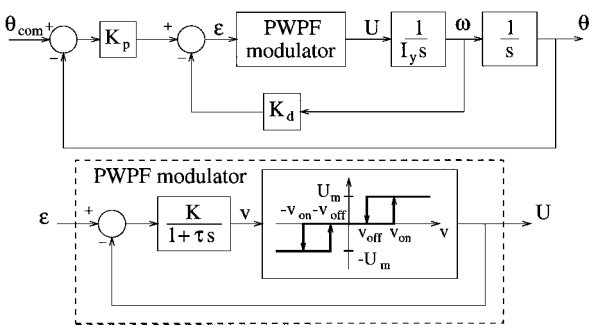

Fig. 3 Block diagram of model 2.

where v is the trigger input. The control torque U is expressed as

$$U = 0, \qquad \text{for} \quad \begin{cases} |v| \le v_{\text{off}} \\ \text{or} \\ v_{\text{off}} < |v| < v_{\text{on}}, \end{cases} \qquad U(t - \delta t) = 0$$

$$U = U_m \operatorname{sign}(v), \qquad \text{for}$$

$$\begin{cases} |v| \ge v_{\text{on}} \\ \text{or} \\ v_{\text{off}} < |v| < v_{\text{on}}, \end{cases} \qquad U(t - \delta t) = U_m \operatorname{sign}[v(t - \delta t)]$$

where U_m is the reaction torque. The state vector is $\boldsymbol{x} = (\omega, \theta, v)$, and the Poincaré map is determined by the analytical integration of set (5), where the Poincaré section is the half-plane defined by $v = 0$, $\omega > 0$. The design parameters of the control system are the network gains, that is, the bandwidth ω_n and damping ζ of the closed-loop system $I_y\ddot{\theta} + K_d\dot{\theta} + K_p\theta = 0$ and the modulator parameters v_{on}, v_{off}, K, and τ.

Analysis

The constant parameters for this application, shown in Table 1, are taken from Ref. 10. As a preliminary observation, the continuation of periodic solutions allows the accurate determination of the oscillation characteristics, that is, limit-cycle amplitude (related to the pointing accuracy) and period T, and of the number of pulses per period and pulse width T_{on}, to evaluate both the fuel consumption (function of the thruster-on time fraction T_{on}/T) and the excitation frequency. Furthermore, continuation of unstable solution branches, when possible, provides detailed information concerning the region of attraction of stable solutions and, therefore, the global stability of the system.

Figure 4 shows a family of bifurcation diagrams of the limit-cycle amplitude $\theta_{\max}$ as a function of ω_n, parameterized with respect to the damping ζ. The curve for $\zeta = 1$ is discussed in detail, to clarify the interpretation of Fig. 4. As the bifurcation parameter is varied in the range 0–50 rad s^{-1} we observe that, in a first interval O–A, globally stable periodic solutions are present where, as ω_n decreases, the limit-cycle amplitude becomes very high. In a second interval A–SN, we have two coexisting branches, that is, locally stable and unstable solutions, and the amplitude of the latter decreases from infinity as the value of ω_n varies from 4 rad s^{-1} (point A) through 38.2 rad s^{-1} (point SN) where a saddle-node bifurcation is visible. Because ω_n is higher than 38.2 rad s^{-1} the system exhibits an oscillatory divergence.

From the kind of results reported in Fig. 4, the stability regions of the system can be represented in the ω_n–ζ plane as shown in Figs. 5 and 6, where the line SN1 is obtained by continuation of the saddle-node bifurcation (SN) as a function of the two variables ω_n and ζ. The second line, A1, separating the local stability region from the global stability region, is traced as the locus of all of the points such as A in Fig. 4, where the asymptote to the unstable branch intersects the ω_n–ζ plane. In Fig. 5, where the lines of constant amplitude of the stable (continuous line) and unstable (dashed line)

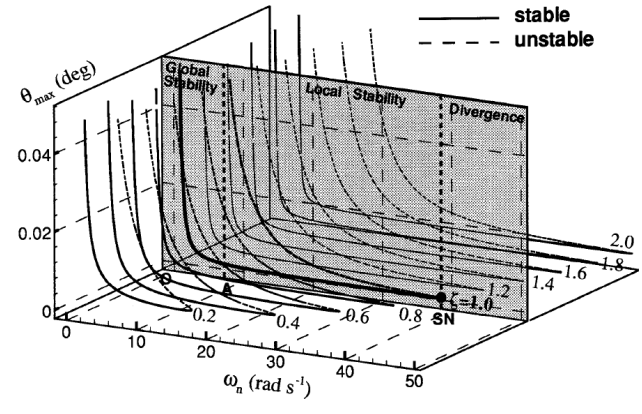

Fig. 4 Model 2: bifurcation diagram of $\theta_{\max}$ vs ω_n at different values of ζ.

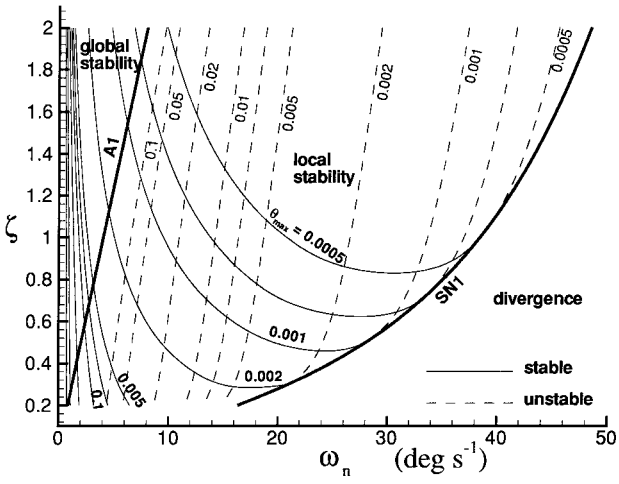

Fig. 5 Stability boundaries in the ω_n–ζ plane.

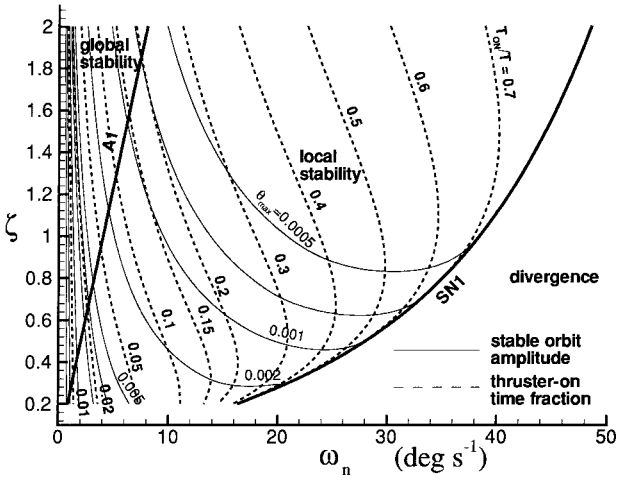

Fig. 6 Stability boundaries in the ω_n–ζ plane.

limit cycles are shown, for any two parameters (ω_n, ζ) we can determine the system stability and the amplitude and attraction domain of the stable orbit (if present). Figure 6 shows, in the ω_n–ζ plane, the lines of constant T_{on}/T and θ_{max} for the stable limit cycles. As already observed in Fig. 4, a sharp increase of the limit-cycle amplitude together with a reduction of the fuel consumption visible in Figs. 5 and 6, respectively, is associated with a small value of ω_n.

For $\zeta < 0.25$, the dynamic behavior of the system is complex. Note that the Poincaré map is locally continuous with respect to variations of the bifurcation parameter λ as long as the number of pulses during an orbit is not varied. When critical values of λ are met, the actual solution disappears, and a new one, with a different number of pulses, is searched for, to identify a new branch of limit cycles. Therefore, as a relevant advantage of the present approach, the bifurcation analysis is not influenced by the number of pulses produced by the modulator. On the other hand, when the dynamic characteristics of the modulator are investigated by DFM, the representation of the modulator output with a single harmonic sinusoid is prevented if more than two opposite pulses per cycle are generated.[3]

In Fig. 7, where the limit-cycle amplitude (Fig. 7a), period (Fig. 7b, continuous lines), and the thruster-on time fraction (Fig. 7b, dashed lines) are shown as a function of ζ, for $\omega_n = 1$ rad s^{-1}, we see several coexisting stable solutions for $0 \le \zeta \le 0.25$ having a different number of pulses. In particular, a higher pulse frequency causes a reduction of both the pointing accuracy and the limit-cycle period and an increment of the fuel consumption.

The complex structure of the domains of attraction of the solutions in Figs. 7 exhibits large variations as ζ is varied in the aforementioned range, and numerical simulation is necessary in this case to characterize the asymptotic behavior of the system for a given initial condition. This is shown in Figs. 8a and 8b, where the regions of

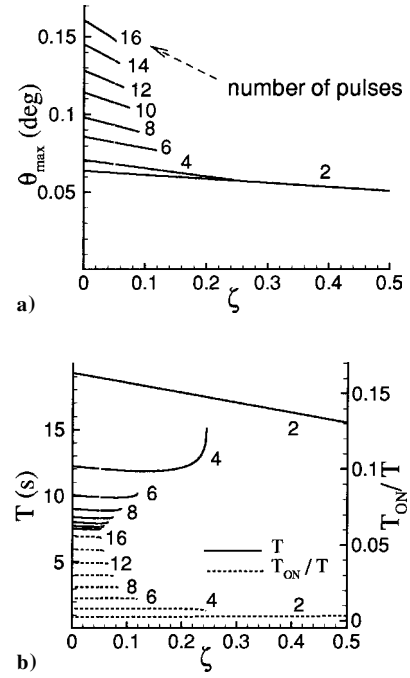

Fig. 7 Model 2: bifurcation diagrams of a) θ_{max} and b) T and T_{on}/T vs ζ.

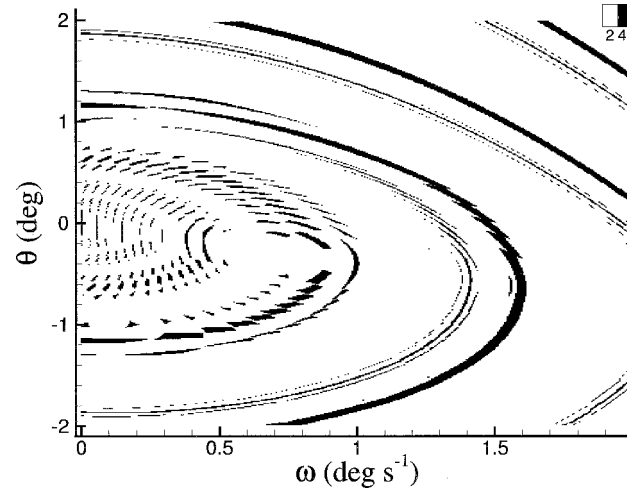

a) $\zeta = 0.2$

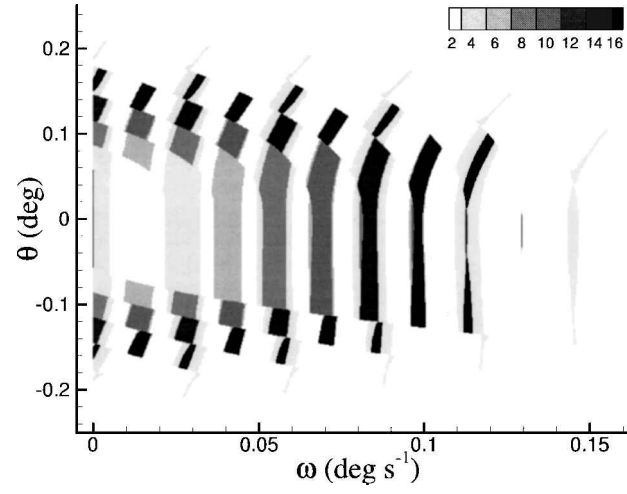

b) $\zeta = 0.05$

Fig. 8 Model 2: domains of attraction on the Poincarè section at $v = 0$.

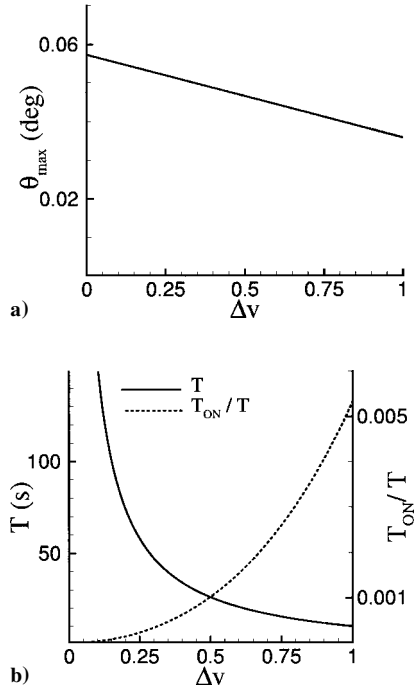

Fig. 9 Model 2: bifurcation diagrams of a) θ_{max} and b) T and T_{on}/T vs $\Delta v = v_{on} - v_{off}$.

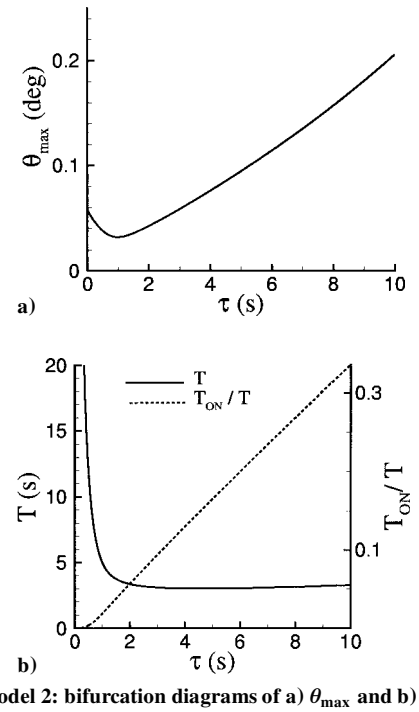

Fig. 10 Model 2: bifurcation diagrams of a) θ_{max} and b) T and T_{on}/T vs τ.

attraction are traced for $\zeta = 0.2$ and 0.05, respectively. In the first case, there are only two competing attractors, whereas eight different limit cycles coexist for $\zeta = 0.05$, with a dramatic increase of θ_{max} and T_{on}/T as the number of pulses per cycle grows. However, in this latter case, the domain of attraction of solutions with more than two pulses per cycle is limited, on the Poincarè section, to low initial values of θ and ω, that is, sizable errors will always cause the system to converge on the limit cycle with favorable characteristics in terms of pointing accuracy and fuel consumption. On the other hand, Fig. 8a shows a different situation, where the domains of attraction of the solutions with two and four pulses per cycle at $\zeta = 0.2$ appear to coexist on the Poincarè section, up to large values of both θ and ω.

For the effects of the modulator parameters, we present the bifurcation diagrams in Fig. 9, where the hysteresis width $\Delta v = v_{on} - v_{off}$, which characterizes the threshold phenomena during the on–off pulse modulation, is selected as bifurcation parameter. The branches in Figs. 9a and 9b, where θ_{max}, T, and T_{on}/T are shown, are traced for $\zeta = 1$, $\omega_n = 1$ rad s^{-1}, and $v_{on} = 1$, and the stable solutions have two pulses. The tradeoff between pointing accuracy and fuel consumption is confirmed, when, for Δv approaching zero, we observe a 30% increase of θ_{max} compared to the nominal condition $\Delta v = 0.9$, whereas the fuel consumption is significantly decreased and the limit-cycle period is much larger. Therefore, provided that the constraints on the pointing accuracy and the thruster on–off cycle are satisfied, a modulator operating at small values of Δv produces a low-frequency pulse command sequence that should be favorable in limiting both the fuel consumption and the excitation of structural modes in flexible spacecraft.

For the influence of the time constant τ, Fig. 10a shows that, in the nominal configuration of Table 1, the pointing accuracy presents a minimum for $\tau = 1$, related to a tradeoff between a slow response for a large value of the time constant and a short-pulse width for $\tau < 1$. The period T in Fig. 10b is equal to 4 s for $\tau = 1$ and, as expected, grows to infinity as the time constant approaches zero, whereas the fuel consumption increases monotonically with τ.

Finally, a variation of the Schmitt trigger on-limit v_{on} from 0 to 15 produces an increase of θ_{max} and T_{on}/T up to 0.6 deg and 6.9, respectively, and has a negligible influence on the limit-cycle period. The effect of the modulator filter gain K appears easily predictable because it is related to the inverse of v_{on}, and it is not discussed.

V. Conclusions

The principal objective of the study was to assess and demonstrate the effectiveness of bifurcation theory and a numerical continuation algorithm for the analysis of nonlinear dynamics in attitude control systems of rigid spacecraft.

The proposed approach based on the continuation of equilibrium points of the Poincaré maps allows for the analysis of systems the nonlinearities of which cannot be reformulated in C^1 form, a situation that is frequently met in spacecraft configurations featuring switching control laws. The reported applications, where single-axis control systems including nonlinear elements are dealt with, show that the qualitative structure of steady states and periodic solutions is revealed, and the effect of several design parameters is efficiently investigated. In comparison with classical techniques such as DFM, the amplitude and frequency of limit cycles are accurately predicted. As a significant advantage, the use of numerical simulation can be limited and, more important, focused onto well-defined regions of the parameter space.

The principal limitation of technique lies in that $\boldsymbol{F}$ is computed by analytical or numerical solution of the equations of motion. This means that the method may not be able to converge onto a new solution during continuation of a highly unstable solution because a new orbit is not detected following perturbation of the initial condition on the Poincaré map. Also, the precise location of the intersections with both the discontinuous manifolds and the Poincaré sections requires an effective numerical procedure because the continuation of the discrete map can be very sensitive to any inaccuracy in the computed trajectory.

In conclusion, provided that the aforementioned issues are addressed, the application of the continuation method to typical satellite configurations confirms that bifurcation theory can be a useful aid in the design of the control system.

Acknowledgment

This work was partially supported by the Italian National Program of Researches in Antarctica.

References

[1] Hess, R. A., and Snell, S. A., "Flight Control System Design with Rate Saturating Actuators," *Journal of Guidance, Control, and Dynamics*, Vol. 20, No. 1, 1997, pp. 90–96.

[2] Gelb, A., and Vender Velde, W. E., *Multiple-Input Describing Functions and Nonlinear System Design*, McGraw–Hill, New York, 1968, pp. 163–185.

[3]Antony, T. C., Wie, B., and Carroll, S., "Pulse-Modulated Control Synthesis for a Flexible Spacecraft," *Journal of Guidance, Control, and Dynamics*, Vol. 13, No. 6, 1990, pp. 1015–1022.

[4]Ferreres, G., and Fromion, V., "Nonlinear Analysis in the Presence of Parametric Uncertainties," *International Journal of Control*, Vol. 69, No. 5, 1998, pp. 695–716.

[5]Guckenheimer, J., and Holmes, P., *Nonlinear Oscillations, Dynamical Systems and Bifurcations of Vector Fields*, Springer-Verlag, New York, 1983, Chaps. 1, 3.

[6]Hirai, K., Iwai, M., and Ushio, T., "Catastrophic Jump Phenomena in a Nonlinear Control System," *IEEE Transactions on Automatic Control*, Vol. AC-26, No. 2, 1981, pp. 601–603.

[7]Cole, J. W., and Calico, R. A., "Nonlinear Oscillations of a Controlled Periodic System," *Journal of Guidance, Control, and Dynamics*, Vol. 15, No. 3, 1992, pp. 627–633.

[8]Piper, G. E., and Kwatny, H. G., "Complicated Dynamics in Spacecraft Attitude Control Systems," *Journal of Guidance, Control, and Dynamics*, Vol. 15, No. 4, 1992, pp. 825–831.

[9]Doedel, E. J., and Kernevez, J. P., "Software for Continuation Problems in Ordinary Differential Equations with Applications," preprint, California Inst. of Technology, Pasadena, CA, 1985.

[10]Voronov, A. A., *Basic Principles of Automatic Control Theory: Special Linear and Nonlinear Systems*, Mir, Moscow, 1985, Chap. 4.

[11]Sidi, M. J., *Spacecraft Dynamics and Control*, Cambridge Univ. Press, New York, 1997, Chap. 9.

[12]Doedel, E., Keller, H. B., and Kervenez, J. P., "Numerical Analysis and Control of Bifurcation Problems—(I) Bifurcation in Finite Dimensions," *International Journal of Bifurcation and Chaos*, Vol. 1, No. 3, 1991, pp. 493–520.

[13]Doedel, E., Keller, H. B., and Kervenez, J. P., "Numerical Analysis and Control of Bifurcation Problems—(II) Bifurcation in Infinite Dimensions," *International Journal of Bifurcation and Chaos*, Vol. 1, No. 4, 1991, pp. 745–772.

[14]Arnol'd, V. I., *Ordinary Differential Equations*, 3rd ed., Springer-Verlag, Berlin, 1992, Chap. 2.

[15]Wiercigroch, M., "Nonlinear Dynamics of Mechanical Systems with Discontinuities," *Proceedings of the IUTAM Symposium on New Applications of Nonlinear and Chaotic Dynamics in Mechanics*, edited by F. C. Moon, Kluwer Academic, Norwell, MA, 1999, pp. 313–322.